



CO<sub>2</sub>  
Human  
Emissions

# Inversion strategy based on OSSEs

Élise Potier, Grégoire Broquet,  
Frédéric Chevallier, Yilong  
Wang, Philippe Ciais

[che-project.eu](http://che-project.eu)



Co-ordinated by  
 ECMWF



# CO<sub>2</sub> Human Emissions

## D3.5 Inversion strategy based on OSSEs

**Dissemination Level:** Public

**Author(s):** É. Potier et al. (CEA/LSCE)

**Date:** 04/02/2021

**Version:** 1.0

**Contractual Delivery Date:** 30/09/2020

**Work Package/ Task:** WP3/ T3.4

**Document Owner:** CEA

**Contributors:** Grégoire Broquet, Frédéric  
Chevallier, Yilong Wang, Philippe Ciais

**Status:** Final



# CO<sub>2</sub> Human Emissions

## CHE: CO<sub>2</sub> Human Emissions Project

Coordination and Support Action (CSA)  
H2020-EO-3-2017 Preparation for a European  
capacity to monitor CO<sub>2</sub> anthropogenic emissions

**Project Coordinator:** Dr Gianpaolo Balsamo (ECMWF)  
**Project Start Date:** 01/10/2017  
**Project Duration:** 39 months

**Published by the CHE Consortium**

**Contact:**

ECMWF, Shinfield Park, Reading, RG2 9AX,  
[gianpaolo.balsamo@ecmwf.int](mailto:gianpaolo.balsamo@ecmwf.int)



The CHE project has received funding from the European Union's Horizon 2020 research and innovation programme under grant agreement No 776186.



## Table of Contents

Executive Summary .....	5
1 Introduction .....	6
1.1 Background.....	6
1.2 Scope of this deliverable .....	6
1.2.1 Objectives of this deliverables.....	6
1.2.2 Work performed in this deliverable .....	6
1.2.3 Deviations and counter measures .....	6
2 Inversion configurations .....	7
2.1 Transport model configuration.....	8
2.2 Transport equations .....	9
2.3 Flux maps and isotopic signatures .....	10
2.3.1 CO <sub>2</sub> and CO fluxes .....	10
2.3.2 Isotopic signatures and <sup>14</sup> CO <sub>2</sub> fluxes.....	10
2.3.3 Ignoring ocean fluxes, cosmogenic production and biomass burning emissions 11	
2.4 Inversion general equation.....	11
2.5 Control Vector.....	11
2.6 Observation vector.....	14
2.7 Prior error covariance matrix B.....	16
2.8 Observation error covariance matrix R.....	17
2.9 Diagnostics .....	17
2.10 Summary of the list of experiments .....	18
3 Results.....	18
4 Conclusion .....	21
Acknowledgements .....	22
5 References .....	22

## Executive Summary

This report presents the high dimensional inversion framework designed for the co-assimilation of CO<sub>2</sub> (from satellite or ground-based measurements) and additional tracers of fossil fuel emissions (CO, <sup>14</sup>CO<sub>2</sub> ground-based observations) and separately controlling emissions from large industrial plants, cities and regional budgets of more diffuse emissions. It currently represents most of north-eastern France, Benelux and western Germany with a ~kilometric resolution. Results are illustrated here about the assimilation of satellite retrievals alone, about the assimilation of ground-based CO<sub>2</sub> and <sup>14</sup>CO<sub>2</sub> measurements, and about the sizeable impact of model error. A larger suite of results is presented and discussed in D4.4, “Sampling Strategy for additional tracers”, in order to contribute to the design of the surface network.

The high-resolution control vector avoids over-optimistic assessment of the capability of observation systems, but involves a very large computational burden. The assimilation of CO and <sup>14</sup>CO<sub>2</sub> is considered separately in order to optimize the computational effort for each tracer. For the CO-CO<sub>2</sub> inversion configuration, we prioritize the control of the different sectors of anthropogenic activity emitting both CO<sub>2</sub> and CO for each target area but we focus on Belgium only. For the <sup>14</sup>CO<sub>2</sub>-CO<sub>2</sub> inversion configuration, we do not need the sectoral resolution and can put the priority on the distinction between various regions around Belgium in the control vector.

Technically, the system requires high performance computing and has been run on a French supercomputer. A <sup>14</sup>CO<sub>2</sub>-CO<sub>2</sub> inversion configuration without radiocarbon involves about ten thousand 24-hour response functions for a 24-hour inversion window. The computation of each response function requires a couple of “wall clock” hours, while other computations in the systems take less than 5 “wall clock” hours. The overall performance could be further optimized for operational use within the future anthropogenic CO<sub>2</sub> emissions Monitoring and Verification Support capacity (CO<sub>2</sub>MVS).

# 1 Introduction

## 1.1 Background

After the Greenhouse Gases Observing Satellite (GOSAT) and second Orbiting Carbon Observatory (OCO-2), the Copernicus Anthropogenic Carbon Dioxide Monitoring (CO<sub>2</sub>M) constellation and its swath of about 300 km of ~ 2x2 km<sup>2</sup> retrievals will represent a new major step in the density of observation of CO<sub>2</sub> and therefore a new challenge for atmospheric inverse modelling systems. The shift from natural CO<sub>2</sub> fluxes to fossil fuel CO<sub>2</sub> emissions will make it even more complicated if the fossil fuel target errors also have kilometre scales, a scientific question that is still debated. In technical terms, the size of the observation vector and the vector of control variables may need to increase considerably from the current situation. These new technical and scientific challenges hamper the evaluation of the future CO<sub>2</sub>M performance and the design of a synergy strategy with other types of observations such as surface measurements of atmospheric tracers linked to CO<sub>2</sub> sources and sinks.

This report documents a high-resolution regional analytical inversion system that was developed for CHE work packages 3 and 4. It currently represents most of north-eastern France, Benelux and western Germany with a ~ kilometric resolution. It can assimilate satellite and in situ observations of CO<sub>2</sub>, CO and radiocarbon, and exploit prior information from inventories to estimate CO<sub>2</sub> emissions at appropriate sectoral-spatio-temporal resolutions. It capitalizes on the expertise of the Laboratoire des Sciences du Climat et de l'Environnement (LSCE) in monitoring urban to regional CO<sub>2</sub> emissions from surface CO<sub>2</sub> observations (Bréon et al., 2015, Staufer et al., 2016, Lian et al., 2019), from high resolution satellite spectro-imagery (ESA 2015, Broquet et al., 2018, Santaren et al., 2020, Wang et al., 2020) and from radiocarbon and CO measurements (Wang 2015, Konovalov et al., 2016, Wang et al., 2016).

After the description of the system, examples of Observing System Simulation Experiments (OSSEs) with satellite observations alone are presented in this report. For this purpose, individual tracks of a CO<sub>2</sub>M-type satellite in Western Europe are considered at local noon. Fossil fuel information is tracked up to 12 hours before, a timescale large enough to represent the typical lifetimes of CO<sub>2</sub> fossil fuel plumes. A larger suite of OSSEs with combined surface-satellite observation scenarios is presented separately in D4.4, "Sampling Strategy for additional tracers", in order to contribute to the design of the surface network in addition to the CO<sub>2</sub>M. Surface observations are assimilated between 10:00 a.m. and 5:00 p.m. local solar time, when the planetary boundary layer is well developed.

## 1.2 Scope of this deliverable

### 1.2.1 Objectives of this deliverables

This report documents a high-resolution regional analytical inversion system that was developed for CHE work packages 3 and 4.

### 1.2.2 Work performed in this deliverable

This deliverable synthesizes the extensive work made by CEA within CHE to design, implement and test a new high-resolution inversion framework.

### 1.2.3 Deviations and counter measures

This deliverable required much more complex modelling work than initially anticipated due to the high resolution of the simulations. The technical challenges related to the massive amount of computation needed for realistic model forward and inverse simulations have therefore slowed progress down and the study extended over four more months than planned.

## 2 Inversion configurations

Within this project, CEA/LSCE has developed a high dimensional inversion framework designed for the co-assimilation of CO<sub>2</sub> and additional tracers of fossil fuel (FF) emissions (CO, <sup>14</sup>CO<sub>2</sub> ground-based observations) and separately controlling emissions from large industrial plants, cities and regional budgets of more diffuse emissions. Such a high-resolution control vector avoids over-optimistic assessment of the capability of observation systems, but involves a very large computational burden. First tests indicated a weak statistical constraint from the CO data. We therefore decided to separately consider the assimilation of CO and <sup>14</sup>CO<sub>2</sub> in order to optimize the computational effort for each tracer. For the “CO-CO<sub>2</sub> inversion configuration”, we prioritize the control of the different sectors of anthropogenic activity emitting both CO<sub>2</sub> and CO (traffic, domestic and commercial heating etc.) for each target area but we focus on Belgium only. For the “<sup>14</sup>CO<sub>2</sub>-CO<sub>2</sub> inversion configuration”, we do not need the sectoral resolution and can put the priority on the distinction between various regions around Belgium in the control vector. The two configurations rely on:

- A regional atmospheric transport model for Western Europe which corresponds to a zoomed configuration of the CHIMERE mesoscale chemistry-transport model (Menut et al. 2013). Our simulation and inversion periods correspond to two days for the CO-CO<sub>2</sub> configuration, one in winter (January 5 2015), the other one in spring (May 11 2015), and 1 day in Summer (July 1 2015) for <sup>14</sup>CO<sub>2</sub>-CO<sub>2</sub> configuration.
- Analytical inversion frameworks (Wu et al., 2016) in which budgets of surface anthropogenic and natural fluxes or auxiliary parameters are controlled at plant, city or regional scales, and at hourly to daily resolution. In the following, the “control” parameters mainly correspond to flux budgets.
- Maps of all type of surface CO<sub>2</sub>, CO and <sup>14</sup>CO<sub>2</sub> fluxes (at temporal resolution up to 1-hour) provided within the project whose plant or city to regional areas are re-scaled by the inversion using daily to hourly scaling factors to better fit the observations.

The inversion tests correspond to OSSEs. We provide observation location, time and corresponding observation uncertainties to the system. However, our analysis relies on the Bayesian framework of the inversions, updating a prior information on the control variables, and on the direct computations of uncertainties in the estimates of the control variables by the analytical systems. Therefore, we do not have to generate values for the synthetic data, and to conduct Monte Carlo experiments to derive the statistics of uncertainties. We analyse the uncertainties in inverted (“posterior”) control parameters as a function of the observation system that is used for the inversion, and the corresponding uncertainty reduction, i.e., the relative difference between the posterior uncertainties and the prior uncertainties in the control parameters.

The basics of the Bayesian inversion theoretical framework have been reminded in the D4.3 CHE report “Attribution Problem Configurations”. The principles, theoretical framework and many parameters of the inversion configurations used here are very close to that used by Santaren et al. (2020) to study the potential of XCO<sub>2</sub> imagery for the monitoring of CO<sub>2</sub> anthropogenic emissions at the regional, city and plant scale. However, in practice, since the inversions here handles the co-assimilation of surface CO, <sup>14</sup>CO<sub>2</sub> and CO<sub>2</sub> data, and since they are based on input products from the CHE projects, they rely on different transport model and analytical inversion configurations. Further details on the inversion concepts and principles relevant for our experiments co-assimilating CO<sub>2</sub> and <sup>14</sup>CO<sub>2</sub> data can be found in Wang (2016).

An important input of the experiments here is the simulation of the CO<sub>2</sub>M XCO<sub>2</sub> sampling during two passes over the area of interest generated by IUPB in the frame of the ESA-PMIF project (Wang et al., 2020, Lespinas et al. 2020).

## 2.1 Transport model configuration

The domain of our CHIMERE transport configuration and for the inversions covers a large part of Western Europe (longitude: -6.82° to 19.18°; latitude: 42.0° to 56.39°). The horizontal resolution of our CHIMERE configuration varies between 50 and 2 km (Figure 1). The 2 km × 2 km-resolution zoom covers Northern France, Luxemburg, Belgium, a large part of the Netherlands and Western Germany (longitude: -1.25° to 10.64°; latitude: 47.45° to 53.15°). The vertical grid is composed of 29 pressure layers extending from 997 hPa to 300 hPa (from the surface to approximately 9km)

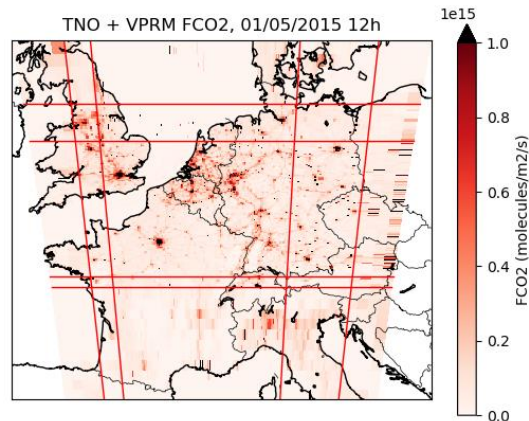


**Figure 1 CO<sub>2</sub> flux map (based on values from the TNO inventory and VPRM simulations for 1 May 2015 at 12:00) over the atmospheric transport modelling grid. The red lines delimit the spatial resolution changes within the domain (from 2 km to 10 km and then 50 km from middle to edges of the domain).**

Our configuration of CHIMERE ignores chemistry since CO<sub>2</sub>, CO and <sup>14</sup>CO<sub>2</sub> are considered as unreactive species at the time scale considered in this study (24h). It is forced by meteorological inputs provided by ECMWF for the WP2. Figure 2 provides indications on the typical horizontal transport conditions during the three days of inversions. On Jan 5 and May 11 the wind is relatively low so that the signal from Belgium should be relatively strong over this country. On July 1 a stronger wind from the North East over the North East part of the domain could spread the atmospheric signatures of FF emissions in the NE-SW direction.

Uncertainties in the initial and boundary conditions are neglected in both CO-CO<sub>2</sub> and <sup>14</sup>CO<sub>2</sub>-CO<sub>2</sub> configurations and, therefore, these conditions themselves are ignored.



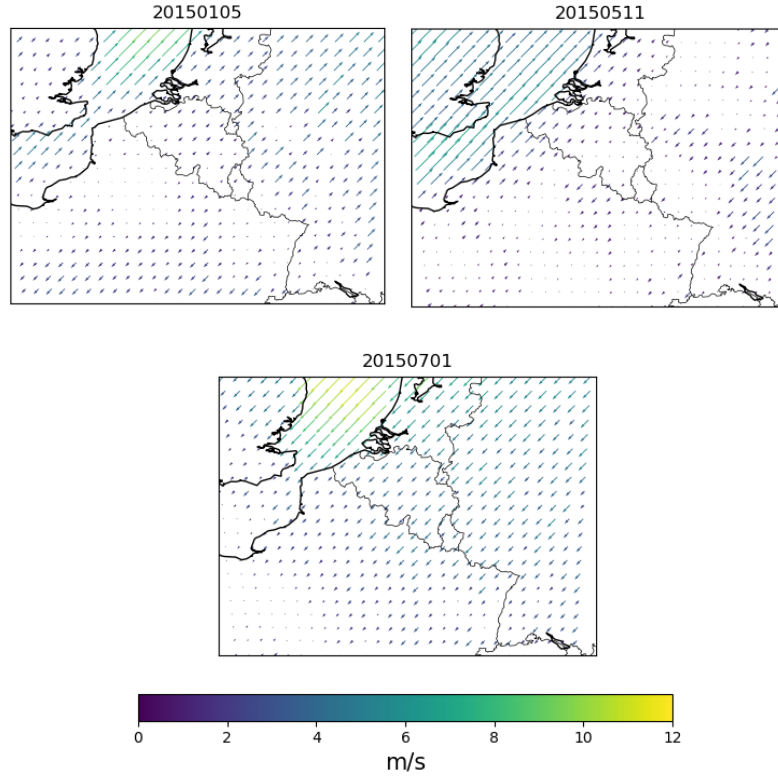


Figure 2 Daily mean wind in the 2<sup>nd</sup> layer of CHIMERE grid (i.e., heights between 25 and 55 m).

## 2.2 Transport equations

We propose a formulation of the transport for CO<sub>2</sub>, CO and <sup>14</sup>CO<sub>2</sub> in our transport and inversion frameworks in order to introduce the notations and our assumptions for the inversion (the formulation of the <sup>14</sup>CO<sub>2</sub> transport follows that of Wang (2016))

$$C_{a,CO_2} = H_{transp} [F_{FF,CO_2} + F_{BF,CO_2} + F_{NPP,CO_2} + F_{HR,CO_2} + F_{ao,CO_2} + F_{oa,CO_2}] + H_{bc} [C_{bc,CO_2}] \quad \text{Eq. (1)}$$

$$C_{a,CO} = H_{transp} [F_{FF,CO} + F_{BF,CO}] + H_{bc} [C_{bc,CO}] \quad \text{Eq. (2)}$$

$$C_{a,CO_2} \delta_a = H_{transp} \begin{bmatrix} \delta_{FF} F_{FF,CO_2} + \delta_{BF} F_{BF,CO_2} + \\ \delta_{NPP} F_{NPP,CO_2} + \delta_{HR} F_{HR,CO_2} + \\ \delta_{ao} F_{ao,CO_2} + \delta_{oa} F_{oa,CO_2} + \\ \frac{1}{R_{std}} F_{Cosm}^{14} + \frac{1}{R_{std}} F_{Nucl}^{14} \end{bmatrix} + H_{bc} [C_{bc,^{14}CO_2} \delta_{bc}], \quad \text{Eq. (3)}$$

where:

- $C_{a,CO_2}$  and  $C_{a,CO}$  are the CO<sub>2</sub> and CO atmospheric concentrations
- $F_x$  terms correspond to different types  $x$  of CO<sub>2</sub> and CO surface fluxes within the transport modelling domain:
  - Fossil fuel emissions (FF)
  - Bio-fuel emissions (BF)
  - Net primary production by vegetation (NPP)
  - Heterotrophic respiration from the soil (HR)

- Exchanges between the ocean and the atmosphere (oa, ao) (neglected in this study, see 3.1.2.3)
- $C_{bc,x}$  are the boundary (top, lateral) and initial conditions of CO<sub>2</sub> and CO and <sup>14</sup>CO<sub>2</sub> concentrations but they are ignored in this inversion study.
- $\delta_a$  are the <sup>14</sup>CO<sub>2</sub>/<sup>12</sup>CO<sub>2</sub> ratios in the atmosphere, normalized by the <sup>14</sup>C/<sup>12</sup>C ratio in the Modern Standard ( $R_{std} = 1.176 \times 10^{-12}$ ). Similarly, in the following, all  $\delta$  are also normalized ratios.
- $\delta_x$  coefficients correspond to the <sup>14</sup>CO<sub>2</sub> abundance in the fluxes listed above.
- $F_{Nucl}^{14}$  correspond to <sup>14</sup>CO<sub>2</sub> fluxes from nuclear power plants (Nucl) and cosmogenic production (cosm, neglected in this study, see 3.1.2.3).

## 2.3 Flux maps and isotopic signatures

### 2.3.1 CO<sub>2</sub> and CO fluxes

The anthropogenic CO<sub>2</sub> and CO emissions, from both FF and BF combustion, are derived from the inventory of the annual emissions produced by TNO for CHE (WP2 and WP4) over Europe for the year 2015 (Denier van der Gon et al., 2017) at ~5 km-resolution (TNO\_GHGco\_v1\_1, longitude -30° to 60°, latitude 30° to 72°; 1/10° × 1/20° resolution) in the CO-CO<sub>2</sub> configuration. In the <sup>14</sup>CO<sub>2</sub>-CO<sub>2</sub> configuration CO<sub>2</sub> emissions are derived from a combination of the two annual inventories produced by TNO for CHE at ~5 km-resolution and at a higher spatial resolution (~2 km) over a smaller domain (TNO\_GHGco\_1x1km\_v1\_1, longitude -2° to 19°, latitude 47° to 56°; 1/60° × 1/120° resolution). These data are projected on the CHIMERE horizontal and vertical grid and at hourly resolution. The vertical (for emissions from point sources only) and temporal disaggregation of the horizontal maps of annual emissions are based on coefficients depending on the sector of activity and considering time zones provided in CHE (see D4.3 CHE report “Attribution Problem Configurations”). Emissions from diffused sectors of activity (traffic, heating etc.) are emitted from the ground in the model.

We use the CO<sub>2</sub> biogenic fluxes provided by MPI-BGC for WP2 and WP4, which are based on simulations with the VPRM model (Vegetation Photosynthesis and Respiration Model, Mahadevan et al., 2008) for the year 2015. These VPRM CO<sub>2</sub> fluxes consist in the Gross Primary Production (GPP) and the respiration (which sums autotrophic and heterotrophic respiration) at hourly resolution and at 5 km × 5 km spatial resolution. We use a daily partition coefficient ( $\alpha_{HR}$ ) to reallocate GPP and Respiration from VPRM into NPP and HR fluxes.

CO biogenic sources are ignored in this study: this could lead to an optimistic assessment of the potential of CO data to support the constraint on anthropogenic emission estimates. However, as stated earlier, the expectations from the first tests regarding the statistical constraint on the CO<sub>2</sub> FF emission estimates from the CO data assimilation were rather low, which did not encourage us to increase the complexity of the CO<sub>2</sub>-CO inversion problem.

### 2.3.2 Isotopic signatures and <sup>14</sup>CO<sub>2</sub> fluxes

This section briefly presents the input data required to simulate the <sup>14</sup>CO<sub>2</sub> transport (see D4.3 CHE report “Attribution Problem Configurations”, for more detail). We use the following  $\delta$  in the fluxes and in the biomass ( $\delta_{biomass}$ ):

- $\delta_{FF} = -1000 \text{ ‰}$ ,
- $\delta_b$ 
  - $\delta_{BF,wood} = 95 \text{ ‰}$  for wood bio-fuel (GNRF categories A to C).
  - $\delta_{BF,crop} = 19 \text{ ‰}$  for crops bio-fuels (GNRF categories F and L).
  - Other types of BF are considered to have negligible emissions.
- $\delta_{NPP}$  monthly maps and  $\delta_{HR}$  daily maps for year 2015.

LSCE provided a <sup>14</sup>CO<sub>2</sub> nuclear emission database as a listing of point source emissions as described in the D4.3 CHE report “Attribution Problem Configurations”. We ignore the temporal variability of these emissions.

### 2.3.3 Ignoring ocean fluxes, cosmogenic production and biomass burning emissions

In the modelling and inversion frameworks, we ignore ocean fluxes, <sup>14</sup>C cosmogenic production and biomass burning emissions, assuming that the impact of the uncertainties in these fluxes are negligible for our analysis.

Regarding CO<sub>2</sub> (and thus <sup>14</sup>CO<sub>2</sub>) ocean fluxes, we assume that they can be neglected because the CHIMERE domain is relatively small and mostly continental <sup>14</sup>CO<sub>2</sub>. The cosmogenic production of <sup>14</sup>C becomes significant above ~700 hPa, well above the planetary boundary layer (Turnbull et al., 2009), while we are interested in simulating <sup>14</sup>CO<sub>2</sub> concentrations near the ground. Even though we use some high-altitude stations, we can assume that most of the influence from cosmogenic production at these surface stations comes from the model lateral boundaries and that the cosmogenic production within the modelling domain can be neglected. CO<sub>2</sub>, <sup>14</sup>CO<sub>2</sub> and CO biomass burning emissions are also neglected since they are generally very low in our modelling domain (especially in the 2-km resolution part of the modelling grid on which the analysis focus) during our months of analysis.

## 2.4 Inversion general equation

Under the assumption that all uncertainties in the inversion problem have a Gaussian and unbiased distribution, these uncertainties are fully characterized by their covariance matrices. The analytical Bayesian inversion allows for the computation of the posterior uncertainty covariance matrix **A** as a function of the observation operator **H** of the covariance matrix of the prior uncertainties **B** and of the model and observation errors covariance matrix **R** (in the observation space) following (Tarantola, 2005):

$$\mathbf{A} = [\mathbf{B}^{-1} + \mathbf{H}^T \mathbf{R}^{-1} \mathbf{H}]^{-1} \quad \text{Eq. (1)}$$

The observation operator **H** connects the control parameters (flux budgets or isotopic signatures) to the observation vector

$$\mathbf{H} = \mathbf{H}_{\text{distr}} \mathbf{H}_{\text{transp}} \mathbf{H}_{\text{sample}} \quad \text{Eq. (2)}$$

Here, it is mainly built on our configuration of the transport model CHIMERE: **H**<sub>transp</sub>. The flux product described in Section 1.2.1 are used to define the spatial and temporal distribution of the fluxes with each control area and beyond the control temporal resolution: **H**<sub>distr</sub>. In practice, the flux budgets in these flux products are also used to scale the prior uncertainty in the control parameters (see below: it’s implied by the definition of the control vector and by the set-up of **B**). **H**<sub>distr</sub> also characterizes the application of the controlled isotopic signatures to CO<sub>2</sub> fluxes.

**H**<sub>sample</sub> corresponds to the computation of XCO<sub>2</sub> or near ground concentrations of CO<sub>2</sub>, CO, <sup>14</sup>CO<sub>2</sub> corresponding to the observations from the 4D fields of CO, CO<sub>2</sub> and <sup>14</sup>CO<sub>2</sub> in output of the CHIMERE model. Section 2.6 provides more details on this operator.

The derivation of the **H** matrix in the analytical system requires an extensive set of simulations with the computation of the signature (column of **H**) of each of the control parameter (Santaren et al., 2020).

## 2.5 Control Vector

The control vector is composed of scaling factors to be applied to local (plant and urban area) to regional budgets from the flux products presented in Section 2.3.1, or to the isotopic signatures presented in Section 2.3.2.

### <sup>14</sup>CO<sub>2</sub>-CO<sub>2</sub> configuration

Within the 24-hour inversion window, the system solves for:

- hourly budgets of the emissions from each large combustion plants in the main area of interest: from FF, wood or crop residue burning
- hourly budgets of 3 types of emissions from large urban areas in the main area of interest and from the regions:
  - FF emissions: diffuse emissions (including that from light combustion plants) for urban areas in the main area of interest, diffuse emissions excluding that of the large urban areas for regions in the main area of interest, and all emissions for regions outside the main area of interest
  - from wood burning (excluding emissions from large plants in the main area of interest)
  - from crop residue burning (excluding emissions from large plants in the main area of interest)
- hourly regional budgets of
  - ecosystem net primary production (NPP)
  - ecosystem heterotrophic respiration (HR)
- the daily  $\delta^{14}\text{C}$  signature of the heterotrophic respiration of ecosystems ( $\delta_{\text{HR}}$ )
- the daily  $\delta^{14}\text{C}$  signature of wood burning  $\delta_{\text{BF,wood}}$  and of crop BFs  $\delta_{\text{BF,crop}}$  emissions
- hourly budgets of the individual nuclear <sup>14</sup>CO<sub>2</sub> fluxes

For anthropogenic (FF and BF) CO<sub>2</sub> emissions and  $\delta_{\text{BF}}$ , the control vector distinguishes 108 urban areas in Luxemburg, in all administrative regions of Belgium, in seven administrative regions of southern Netherlands, in three administrative regions in northern France and three administrative regions in western Germany (all comprised in the 2 km × 2 km-resolution zoom of the CHIMERE grid, see Figure 3). This set of regions is called “the main area of interest” hereafter. In these administrative regions, the CO<sub>2</sub>/<sup>14</sup>CO<sub>2</sub> emissions from major industrial plants (22 plants > 1 MtonC for CO<sub>2</sub> and 47 nuclear power plants for <sup>14</sup>CO<sub>2</sub>) are also controlled separately. The inversions also control separately the rest of the emissions in each of these administrative regions.

Outside this detailed area, and for France, Germany and Netherlands, the inversion controls the full budget of FF and BF (distinguishing between wood and crop burning) CO<sub>2</sub> emissions and of nuclear <sup>14</sup>CO<sub>2</sub> emissions over the administrative regions (Figure 4). Coarser areas of control for the anthropogenic emissions are used for the rest of the domain.

Biogenic fluxes and isotopic signatures (NPP, HR and  $\delta_{\text{HR}}$ ) are only controlled at the resolution of administrative regions and larger area (Figure 4), i.e., the spatial resolution of the control vector is nearly the same as for anthropogenic emissions but it does not isolate urban areas and major point sources.

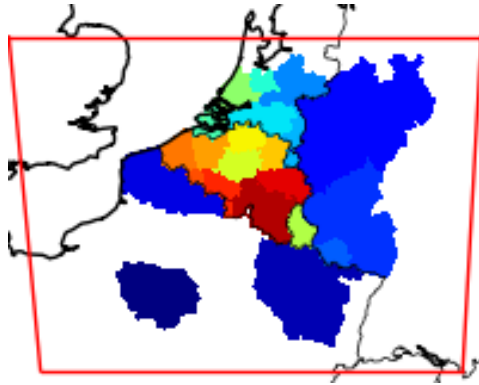


**Figure 3** Main area of interest i.e. the administrative regions where urban areas and point sources emissions are controlled separately in the <sup>14</sup>CO<sub>2</sub>-CO<sub>2</sub> inversion configuration. The red line delimits the 2 km × 2 km-resolution zoom of the CHIMERE transport model.

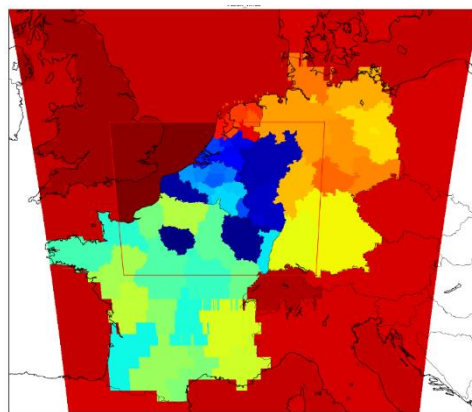


**Figure 4** Administrative regions and coarser areas for which the biogenic flux budgets, and the anthropogenic emission budget (with more details for regions highlighted in Figure 3), are controlled in the <sup>14</sup>CO<sub>2</sub>-CO<sub>2</sub> inversion configuration. The red line delimits the 2 km × 2 km-resolution zoom of the CHIMERE transport model.

### CO-CO<sub>2</sub> configuration

The proper co-assimilation of CO and CO<sub>2</sub> data requires the separate control of FF and BF anthropogenic emissions for the different main sectors of emitting activities. The CO-CO<sub>2</sub> inversion configuration relies on the same CHIMERE configuration as the <sup>14</sup>CO<sub>2</sub>-CO<sub>2</sub> inversion configuration, but its control vector, its observation vector and the corresponding analysis are focused on Belgium. The control vector gathers ten areas of control only (nine in Belgium, and one for the rest of the domain, Figure 5), but the resolution of the FF and BF emissions is split between six emission sectors to be controlled separately in each of the corresponding region at 1-hour resolution (Table 1). The hourly budgets of the NEE (Net Ecosystem Exchange: NPP+HR) are directly controlled (instead of the budgets of NPP and HR as in the <sup>14</sup>CO<sub>2</sub>-CO<sub>2</sub> inversion configuration) in the 10 controlled areas.

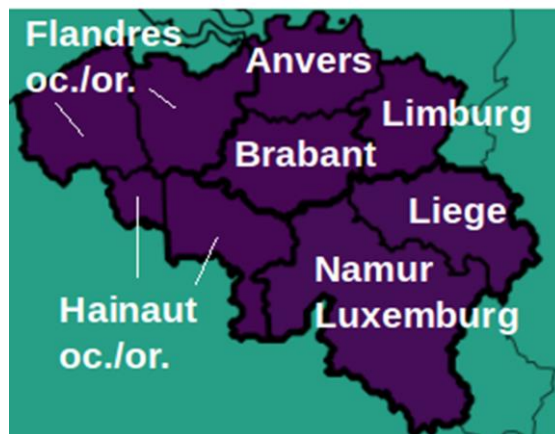


Figure 5 Controlled areas in the CO-CO<sub>2</sub> inversion configuration: nine Belgium administrative regions and the rest of the domain.

Table 1 Controlled sectors of emitting activities in the CO-CO<sub>2</sub> inversion configuration

	Name	GNFR category in TNO inventories
1	Public power	A_PublicPower
2	Industry (+solvents and fugitives)	B_Industry D_Fugitives E_solvents
3	Stationary combustion	C_OtherStationaryComb
4	Transport (no diesel)	F_RoadTransport_exhaust_gasoline F_RoadTransport_exhaust_LPG_gas F_RoadTransport_exhaust_non-exhaust
5	Transport (diesel)	F_RoadTransport_exhaust_diesel
6	Other	G_Shipping H_Aviation I_OffRoad J_Waste K_AgriLivestock L_AgrisOther

## 2.6 Observation vector

Different configurations of the observation system are tested for the 1-day inversions, combining one satellite pass and/or ground-based observation stations measuring CO<sub>2</sub> and/or CO/<sup>14</sup>CO<sub>2</sub> data.

For the CO-CO<sub>2</sub> inversion configuration, the observation vector is restricted to the Belgium area.

### Satellite observations from an XCO<sub>2</sub> spectro-imager such as CO2M

In both CO-CO<sub>2</sub> and <sup>14</sup>CO<sub>2</sub>-CO<sub>2</sub> inversion configurations, the simulation of CO<sub>2</sub> satellite observations is based on the simulations of the CO2M sampling and L2-errors in the surface and atmospheric conditions of the year 2014 by IUPB in the ESA-PMIF project (Wang et al., 2020, Lespinas et al. 2020). These simulations account for cloud cover. Two passes over the area of interest from this product are used in our experiments, with a moderate cloud coverage (Figure 6 and Figure 7). We assume that the overpasses occur at 12:00. The observation vector is defined by the individual cloud free pixels of the satellite. The extraction of this observation vector from the model is made by selecting the model grid cells in which the centres of these satellite cloud free pixels are located. The spatial resolution of our transport model in the area of interest is similar to that of the CO2M observation (2 km). However, since the satellite ground pixels do not perfectly overlap the model grid cells in this area, some model grid cells can correspond to several observations. In the coarser part of the model grid, many model grid cells correspond to several observations (Figure 7).

The integrated column of CO<sub>2</sub> (XCO<sub>2</sub>) is computed from the CHIMERE 3D fields of CO<sub>2</sub> based on the following equation:

$$X_{CO_2} = \frac{(\sum_{l=0}^{nl} (P^{l+1} - P^l) \times CO_2^l) - CO_2^{nl+1} \times P^{nl}}{-P^0} \quad \text{Eq. (3)}$$

where P is the atmospheric pressure at the surface (P<sup>0</sup>) or in the layer l (P<sup>l</sup>), nl is the number of layers in the simulation vertical grid, CO<sub>2</sub><sup>l</sup> are the corresponding CO<sub>2</sub> concentrations in each layer and CO<sub>2</sub><sup>nl+1</sup> corresponds to the horizontal average of the top-level mixing ratios in CHIMERE.

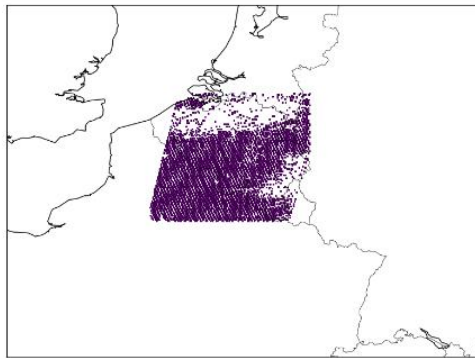


**Figure 6 Selected CO2M track 1, restricted to the vicinity of Belgium, for the CO-CO<sub>2</sub> inversion configuration.**

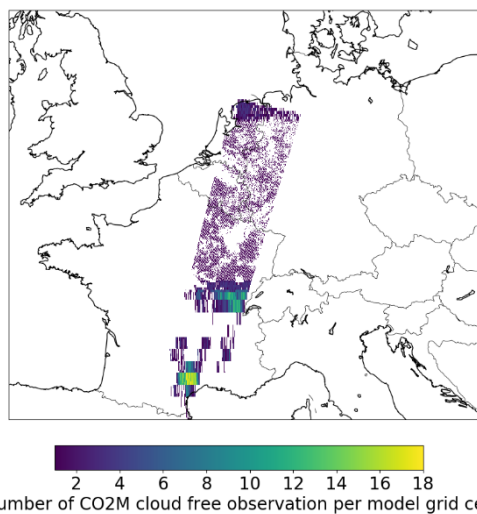


**Figure 7 Selected CO2M track 2 for the <sup>14</sup>CO<sub>2</sub>-CO<sub>2</sub> inversion configuration.**

### Ground-based networks

Two sets of station locations are used: one for CO-CO<sub>2</sub> inversion configuration, one for the <sup>14</sup>CO<sub>2</sub>-CO<sub>2</sub> inversion configuration. We assume that all stations of these networks measure simultaneously CO<sub>2</sub> and/or CO (in the CO-CO<sub>2</sub> inversion configuration) / <sup>14</sup>CO<sub>2</sub> (in the <sup>14</sup>CO<sub>2</sub>-CO<sub>2</sub> inversion configuration).

The network used for the CO-CO<sub>2</sub> inversion configuration focused on Belgium is denser than the one proposed in D4.3 CHE report “Attribution Problem Configurations” (the lack of constraint on FF CO<sub>2</sub> emissions from the CO data in initial tests pushed for testing such an increased density) in the area with 5 stations in Belgium and 5 around (Figure 8, left). The height of all the stations corresponds to the second vertical layer of the transport model (i.e., to heights between 25 and 55 m). The stations provide hourly averages of CO and/or CO<sub>2</sub>. Following a traditional practice in inversions at global to city scales (Bréon et al., 2015) we only assimilate data when the planetary boundary layer (PBL) is well developed and the

vertical mixing in transport models is not a major source of bias near the surface: in practice, here, hourly averages between 10:00 and 17:00 in the CO-CO<sub>2</sub> inversion configuration.

The network used for the <sup>14</sup>CO<sub>2</sub>-CO<sub>2</sub> inversion configuration (Figure 8, right). is the one proposed in the D4.3 CHE report “Attribution Problem Configurations”. It includes 113 stations in our domain whose heights range between 10 and 344 m. Each site provides hourly CO<sub>2</sub> data that are assimilated between 10:00 and 17:00 only and/or 7-hour average sample of <sup>14</sup>CO<sub>2</sub> over 10:00-17:00 (following, again, the common practice of assimilating data only when the PBL is well developed).

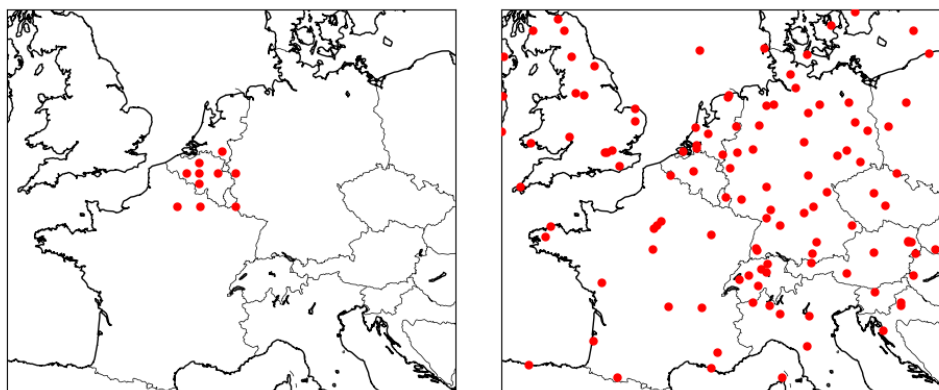


Figure 8 ground-based CO/CO<sub>2</sub> (left) and <sup>14</sup>CO<sub>2</sub>/CO<sub>2</sub> (right) observation networks

## 2.7 Prior error covariance matrix B

**B** is built assuming:

- 3-hour temporal auto-correlation of the prior uncertainty in hourly budgets for any type of controlled fluxes: an exponentially decaying function ( $e^{-d/3h}$ , where  $d$  is the time lag between two hourly fluxes) is used to model these temporal correlations.
- that there is no correlation of the prior uncertainties in space, between sectors of the anthropogenic emissions, or between different types of fluxes of a given species
- a correlation of 0.8 between prior uncertainties in CO and CO<sub>2</sub> anthropogenic FF or BF emissions (in the CO-CO<sub>2</sub> inversion configuration) for any sector of activity. This correlation provides the critical link between the co-emitted species. 0.8 is probably a high value which sounds optimistic regarding the ability to cross information between CO and CO<sub>2</sub> (D4.3 CHE report “Attribution Problem Configurations”).

In the CO-CO<sub>2</sub> inversion configuration, the prior uncertainty in CO<sub>2</sub> and CO FF and BF 24-h budget is set to 30 % and that in CO<sub>2</sub> NEE is set to 60%. The disaggregation of these uncertainties into prior uncertainties in individual control parameters (hourly budgets of fluxes) is based on the assumptions regarding the correlations detailed above.

The configuration of the prior uncertainties in the <sup>14</sup>CO<sub>2</sub>-CO<sub>2</sub> inversion configuration at daily scale are provided in Table 2.

**Table 2 Standard deviations of the prior uncertainties in 24-h budgets of fluxes or in isotopic signatures for each control area in the <sup>14</sup>CO<sub>2</sub>-CO<sub>2</sub> inversion configuration**

	FF_PS	FF_other	BF_crop	BF_wood	NPP	HR	delta_BF_cr op	delta_BF_wo od	delta_HR	nucl
Prior uncertainties	30 %	30 %	30 %	30 %	60%	60%	100%	100%	100%	100%



**Table 3 Range of standard deviations of the prior uncertainties in regional 24-h, morning and afternoon budgets of FF emissions in the main area of interest in the <sup>14</sup>CO<sub>2</sub>-CO<sub>2</sub> inversion configuration. These budgets include the urban areas and point sources within the regions.**

Prior uncertainty in regional budget %	24-h	Morning	Afternoon
Min	10	15	16
Mean	20	29	31
Max	30	43	45

## 2.8 Observation error covariance matrix R

The matrix **R** combines uncertainties in the data that are assimilated and the corresponding uncertainties from the observation operator. Here we assume that the uncertainties from the observation operator are dominated by that of the transport model. We ignore temporal and spatial auto-correlations in these uncertainties. For individual data:

$$\varepsilon_{Obs} = \sqrt{\varepsilon_{meas.}^2 + \varepsilon_{mod}^2} \quad \text{Eq. (4)}$$

The typical error on CO<sub>2</sub>M XCO<sub>2</sub> data simulated by IUPB in our area of interest is 0.6 ppm. We use this value of uncertainty for all the individual data of both tracks. The corresponding model error is taken as 1 ppm (Basu et al. 2018).

The configuration of the observation errors for the near surface CO<sub>2</sub>, CO and <sup>14</sup>CO<sub>2</sub> data follows the guidelines of section 5 of the D4.3 CHE report “Attribution Problem Configurations” (Tables 5-1 to 5-3). Conversions of model error for the <sup>14</sup>CO<sub>2</sub> data are done assuming a CO<sub>2</sub> atmospheric concentration of 400 ppm and an atmospheric δ<sub>14C,a</sub> of 40 ‰. For all sites, we use the model error that the D4.3 CHE report proposed for continental stations (Table 5-3). The corresponding values are reported in Table 3. Since auto correlations are ignored for the model error at the hourly scale, the model error for 7-hour averages of <sup>14</sup>CO<sub>2</sub> concentrations is taken as 1/√7 times the model error at the 1-hour scale.

Table 4 Measurement and model errors

Error	Near-surface		Satellite	
	Meas.	Model	Meas.	Model
CO <sub>2</sub> (ppm)	0.1	3	0.6	1
CO (ppb)	5	21		
<sup>14</sup> CO <sub>2</sub> (ppm ‰)	800*	1214**		

$$* \sqrt{(CO_2 \times \sigma_{\delta_{14C,obs}})^2 \times (\delta_{14C,a} \times \sigma_{CO_2,obs})^2} = \sqrt{(400 \times 2)^2 \times (40 \times 0.1)^2}$$

\*\* conversion  $3 \times \sigma^{14CO_2,model} / Rstd \times 1000 / \sqrt{7} = 3 \times 1.26 / 1.176 \times 1000 / \sqrt{7} = 1214$  ppm permil, with  $\sigma_{\delta_{14C,obs}}$ ,  $\sigma_{CO_2,obs}$  and  $\sigma_{14CO_2,model}$  as defined in Tables 5-1 and 5-2 of CHE D4.3

## 2.9 Diagnostics

When analysing the results from the inversion and assessing the potential of the different types of observation networks, we focus on the standard deviation (STD) of the prior and posterior uncertainties in flux budgets, and on their relative difference (called uncertainty reduction or UR hereafter):

$$UR = 1 - \frac{\sigma_{post}}{\sigma_{prior}} \quad \text{Eq. (5)}$$

Hereafter, when analysing temporal budgets of uncertainties, “morning” and “afternoon” are used to designate 6:00-13:00 and 13:00-19:00 respectively. Our analyses are focused on budgets for regions in the 2-km-resolution area and more particularly in the main area of interest as defined in Figure 3.

## 2.10 Summary of the list of experiments

The following Table 5 provides labels for the different performed experiments most of them are analysed in the D4.4, “Sampling Strategy for additional tracers” and some of them are presented afterwards.

Table 5 Experiment labels

Inversion system Observations	Europe: <sup>14</sup> CO <sub>2</sub> -CO <sub>2</sub> inversion configuration on 1 <sup>st</sup> of July 2015	Belgium: CO-CO <sub>2</sub> inversion configuration on 5 <sup>th</sup> of January 2015 or on 11 <sup>th</sup> of May 2015
Satellite XCO <sub>2</sub>	EUR-Sat	BE-Sat
Surface CO <sub>2</sub>	EUR-CO <sub>2</sub>	BE-CO <sub>2</sub>
Satellite XCO <sub>2</sub> + Surface CO <sub>2</sub>	EUR-Sat-CO <sub>2</sub>	BE-Sat-CO <sub>2</sub>
Surface <sup>14</sup> CO <sub>2</sub>	EUR- <sup>14</sup> CO <sub>2</sub>	no
Satellite XCO <sub>2</sub> + Surface <sup>14</sup> CO <sub>2</sub>	EUR-Sat- <sup>14</sup> CO <sub>2</sub>	no
Surface CO <sub>2</sub> + Surface <sup>14</sup> CO <sub>2</sub>	EUR-CO <sub>2</sub> - <sup>14</sup> CO <sub>2</sub>	no
Satellite XCO <sub>2</sub> + Surface CO <sub>2</sub> and <sup>14</sup> CO <sub>2</sub>	EUR-Sat-CO <sub>2</sub> - <sup>14</sup> CO <sub>2</sub>	no
Surface CO	no	BE-CO
Satellite XCO <sub>2</sub> + Surface CO <sub>2</sub> and CO	no	BE-Sat-CO <sub>2</sub> -CO

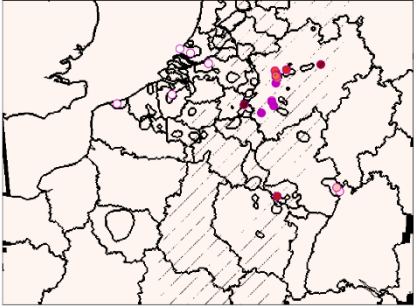
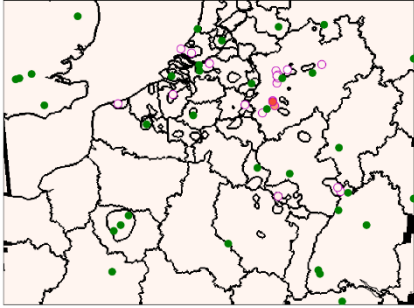
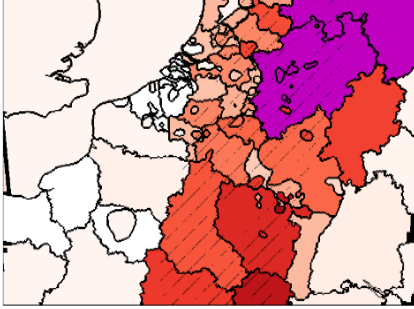
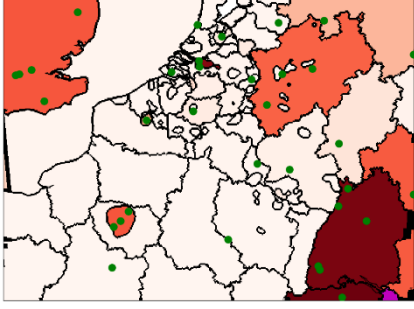
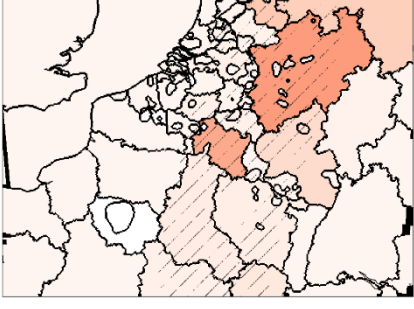
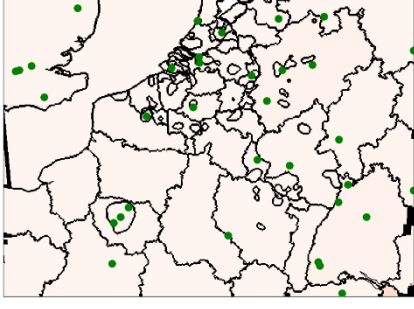
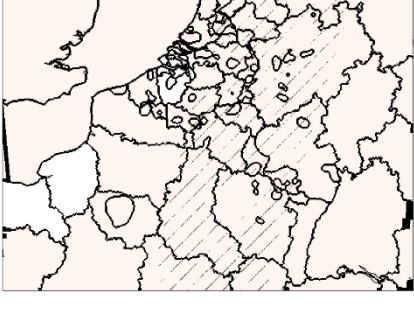
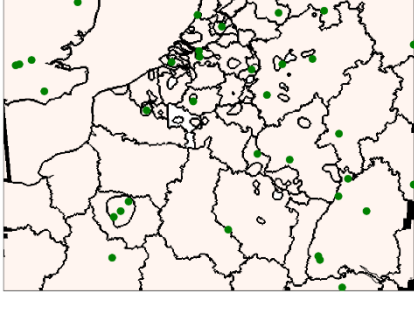
Further sensitivity tests are conducted by setting the prior uncertainties in NEE and BF fluxes to 0 (i.e. ignoring these fluxes) but we do not explicitly label them.

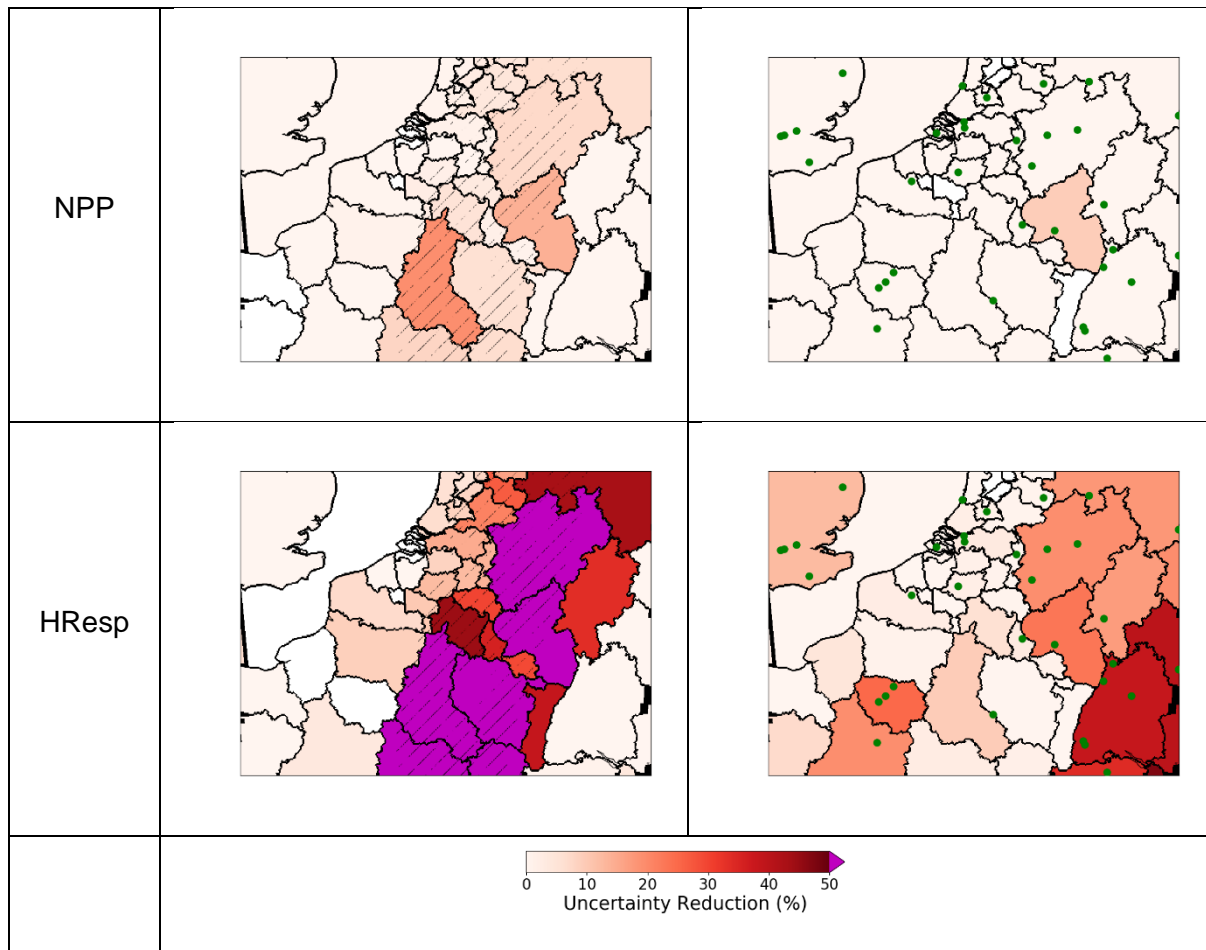
## 3 Results

This section illustrates the capability of the inversion systems. A more extensive set of results is presented and discussed in D4.4, “Sampling Strategy for additional tracers”, in order to contribute to the design of the surface network.

Figure 9 shows an example panel of UR in two inversion configurations (EUR-Sat and EUR-CO<sub>2</sub>-<sup>14</sup>CO<sub>2</sub>, as defined in Table 5), for morning budget of CO<sub>2</sub> fluxes, from the point source scale to the region scale according to the controlled fluxes (large plant emissions, other FF and BF emissions and biogenic flux components). The UR on the morning budget of large plants is significant in the satellite ground coverage, with values higher than 50% (Figure 9, FF\_PS a) and marginal outside the satellite coverage despite the north-eastern wind (see Section 2.1). The impact of the ground network depends on the station location (Figure 9, FF\_PS b) with significant UR for only two large plants in western Germany. UR are also significant for other fossil fuel emission budgets (FF\_other) and Heterotrophic respiration (HResp) in the satellite coverage (a) and in region with stations (b) with UR until 50% and more. UR are lower for BF emission and NPP fluxes morning budgets.

UR	a	b
	EUR-Sat	EUR-CO <sub>2</sub> - <sup>14</sup> CO <sub>2</sub>

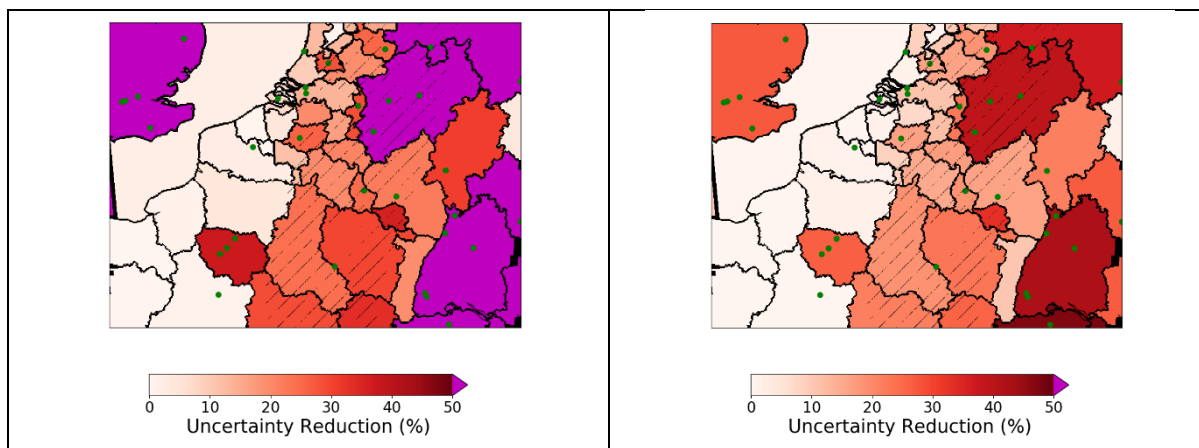
Morning budgets		
FF_PS		
FF_other		
BF_Wood		
BF_Crop		



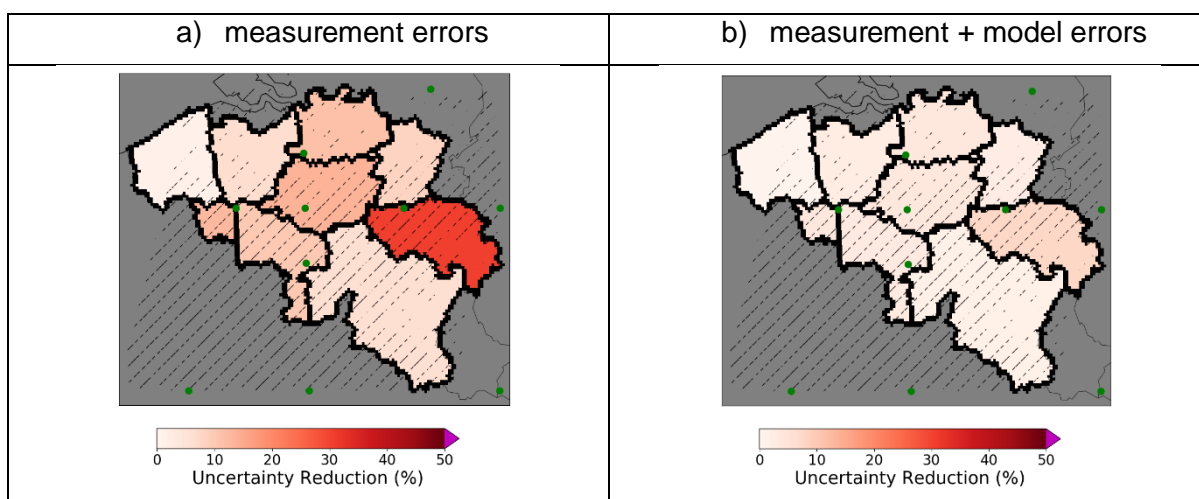
**Figure 9** Uncertainty reduction in EUR-Sat and EUR-CO<sub>2</sub>-<sup>14</sup>CO<sub>2</sub> inversions: for morning budgets of large plants (FF\_PS, magenta circled dots), other FF and BF (crop and wood) emissions (urban area and rest of the region budgets), Net Primary Production (NPP) and heterotrophic respiration (HR) (regional budgets). Stripes indicate the satellite coverage. Green dots indicate the ground stations.

Figure 10 and Figure 11 highlight the importance of considering the model error in both the CO-CO<sub>2</sub> inversion configuration and the <sup>14</sup>CO<sub>2</sub>-CO<sub>2</sub> one. Indeed, the model error impact is sizeable and uncertainty reductions are overestimated when this source of uncertainty is not neglected. In Figure 10 (EUR-Sat-CO<sub>2</sub>-<sup>14</sup>CO<sub>2</sub> inversion), the UR for daily budgets of FF emissions are often larger than 50 % without model error (a) while they are significantly lower with the model error (b). In Figure 11 (BE-CO<sub>2</sub>-CO inversion), the differences are also significant with around 10 percentage points of difference. The differences seem to be particularly strong in the regions with ground stations, highlighting the impact of the model errors at stations. However, well assigning the model error statistics remains challenging.

a) measurement errors	b) measurement + model errors
-----------------------	-------------------------------



**Figure 10** Uncertainty reduction in EUR-Sat-CO<sub>2</sub>-<sup>14</sup>CO<sub>2</sub> inversion: for daily budgets of FF emissions, with data measurement errors only (a) and with both data measurement errors and observation operator errors (model errors) (b). Stripes indicate the satellite coverage. Green dots indicate the ground stations.



**Figure 11** Uncertainty reduction in the BE-CO<sub>2</sub>-CO inversion: for daily budgets of FF emissions, with data measurement errors only (a) and with both data measurement errors and observation operator errors (model errors) (b). Stripes indicate the satellite coverage. Green dots indicate the ground stations.

## 4 Conclusion

This report presents the high dimensional inversion framework designed for the co-assimilation of CO<sub>2</sub> (from satellite or ground-based measurements) and additional tracers of fossil fuel emissions (CO, <sup>14</sup>CO<sub>2</sub> ground-based observations) and separately controlling emissions from large industrial plants, cities and regional budgets of more diffuse emissions. It currently represents most of north-eastern France, Benelux and western Germany with a ~kilometric resolution. Results are illustrated here about the assimilation of satellite retrievals alone, about the assimilation of ground-based CO<sub>2</sub> and <sup>14</sup>CO<sub>2</sub> measurements, and about the sizeable impact of model error. A larger suite of results is presented and discussed in D4.4, “Sampling Strategy for additional tracers”, in order to contribute to the design of the surface network.

The high-resolution control vector avoids over-optimistic assessment of the capability of observation systems, but involves a very large computational burden. The assimilation of CO and <sup>14</sup>CO<sub>2</sub> is considered separately in order to optimize the computational effort for each tracer. For the CO-CO<sub>2</sub> inversion configuration, we prioritize the control of the different sectors of anthropogenic activity emitting both CO<sub>2</sub> and CO for each target area but we focus on Belgium only. For the <sup>14</sup>CO<sub>2</sub>-CO<sub>2</sub> inversion configuration, we do not need the sectoral resolution and can put the priority on the distinction between various regions around Belgium in the control vector.

Technically, the system has been run on supercomputer Irene-Skylake of Très Grand Centre de Calcul of CEA (TGCC, <http://www-hpc.cea.fr/en/complexe/tgcc.htm>). Irene-Skylake is made of Intel Xeon 8168 (SKL) bi-processor nodes with 2.7-GHz cores and with 192 GB of DDR4 memory for each node. The <sup>14</sup>CO<sub>2</sub>-CO<sub>2</sub> inversion configuration involves 15,768 24-hour response functions for a 24-hour inversion window. One third of these response functions is for radiocarbon only and are not needed when only CO<sub>2</sub> observations are assimilated. When response functions are computed with 5 cores (one master and four slaves), the observed “wall clock” computing time on Irene-Skylake ranges between 1.5 and 4.25 hours for each one. Additional time for meteorological and CO<sub>2</sub> emission pre-processing is comparatively negligible. The inversion itself and post processing can be achieved in less than 3 hours. The overall performance could be further optimized, but already provides an idea of the computational burden of the full inversion system (including the computation of the response functions): it is substantial and addresses a portion of western Europe only, but may not be out of reach in the near future, given possible technical improvements (like, obviously, the transfer of some of the computation on GPU), for an operational system that would process CO<sub>2</sub>M operational data over some fossil-fuel emission regions of interest, in addition to providing OSSE diagnostic results easily once the response functions have been computed.

## Acknowledgements

The simulation of CO<sub>2</sub>M XCO<sub>2</sub> samplings over the area of interest has been generated by IUP-UB in the framework of the ESA PMIF project.

## 5 References

Basu, S., Baker, D. F., Chevallier, F., Patra, P. K., Liu, J., and Miller, J. B.: The impact of transport model differences on CO<sub>2</sub> surface flux estimates from OCO-2 retrievals of column average CO<sub>2</sub>, *Atmos. Chem. Phys.*, 18, 7189–7215, <https://doi.org/10.5194/acp-18-7189-2018>, 2018.

Denier van der Gon, Hugo A. C., Jeroen J. P. Kuenen, Greet Janssens-Maenhout, Ulrike Döring, Sander Jonkers, et Antoon Visschedijk. 2017. « TNO\_CAMS High Resolution European Emission Inventory 2000–2014 for Anthropogenic CO<sub>2</sub> and Future Years Following Two Different Pathways ». *Earth System Science Data Discussions*, novembre, 1-30. <https://doi.org/10.5194/essd-2017-124>.

Lespinas, Franck, Yilong Wang, Grégoire Broquet, François-Marie Bréon, Michael Buchwitz, Maximilian Reuter, Yasjka Meijer, et al. 2020. « The potential of a constellation of low earth orbit satellite imagers to monitor worldwide fossil fuel CO<sub>2</sub> emissions from large cities and point sources ». *Carbon Balance and Management* 15 (1): 18. <https://doi.org/10.1186/s13021-020-00153-4>.

Lian, J., Breon, F.-M., Broquet, G., Zheng, B., Ramonet, M., & Ciais, P. (2020). Quantitative evaluation of the uncertainty sources for the modeling of atmospheric CO<sub>2</sub> concentration

within and in the vicinity of Paris city. *Atmospheric Chemistry and Physics Discussions*, 1–22. <http://doi.org/10.5194/acp-2020-540>

Mahadevan, Pathmathevan, Steven C. Wofsy, Daniel M. Matross, Xiangming Xiao, Allison L. Dunn, John C. Lin, Christoph Gerbig, J. William Munger, Victoria Y. Chow, et Elaine W. Gottlieb. 2008. « A Satellite-Based Biosphere Parameterization for Net Ecosystem CO<sub>2</sub> Exchange: Vegetation Photosynthesis and Respiration Model (VPRM) ». *Global Biogeochemical Cycles* 22 (2). <https://doi.org/10.1029/2006GB002735>.

Menut, L., B. Bessagnet, D. Khvorostyanov, M. Beekmann, N. Blond, A. Colette, I. Coll, et al. 2013. « CHIMERE 2013: A Model for Regional Atmospheric Composition Modelling ». *Geoscientific Model Development* 6 (4): 981-1028. <https://doi.org/10.5194/gmd-6-981-2013>.

Santaren, Diego, Grégoire Broquet, François-Marie Bréon, Frédéric Chevallier, Denis Siméoni, et Philippe Ciais. 2020. « A Local to National-Scale Inverse Modeling System to Assess the Potential of Spaceborne CO<sub>2</sub> Measurements for the Monitoring of Anthropogenic Emissions ». *Atmospheric Measurement Techniques Discussions*, mai, 1-41. <https://doi.org/10.5194/amt-2020-138>.

Stauffer, J., Broquet, G., Breon, F.-M., Puygrenier, V., Chevallier, F., Xueref-Remy, I., et al. (2016). The first 1-year-long estimate of the Paris region fossil fuel CO<sub>2</sub> emissions based on atmospheric inversion. *Atmospheric Chemistry and Physics*, 16(22), 14703–14726. <http://doi.org/10.1029/2005JD006003>

Tarantola, Albert. 2005. *Inverse Problem Theory and Methods for Model Parameter Estimation*. Society for Industrial and Applied Mathematics. <https://doi.org/10.1137/1.9780898717921>.

Turnbull, Jocelyn, Peter Rayner, John Miller, Tobias Naegler, Philippe Ciais, et Anne Cozic. 2009. « On the Use of <sup>14</sup>CO<sub>2</sub> as a Tracer for Fossil Fuel CO<sub>2</sub>: Quantifying Uncertainties Using an Atmospheric Transport Model ». *Journal of Geophysical Research: Atmospheres* 114 (D22). <https://doi.org/10.1029/2009JD012308>.

Wang, Peng, Weijian Zhou, Zhenchuan Niu, Peng Cheng, Shugang Wu, Xiaohu Xiong, Xuefeng Lu, et Hua Du. 2018. « Emission characteristics of atmospheric carbon dioxide in Xi'an, China based on the measurements of CO<sub>2</sub> concentration, Δ<sup>14</sup>C and δ<sup>13</sup>C ». *Science of The Total Environment* 619-620 (avril): 1163-69. <https://doi.org/10.1016/j.scitotenv.2017.11.125>.

Wang, Yilong. 2016. « The Potential of Observations of Radiocarbon in Atmospheric CO<sub>2</sub> for the Atmospheric Inversion of Fossil Fuel CO<sub>2</sub> Emission at Regional Scale », novembre. <https://tel.archives-ouvertes.fr/tel-01529200>.

Wang, Yilong, Grégoire Broquet, François-Marie Bréon, Franck Lespinas, Michael Buchwitz, Maximilian Reuter, Yasjka Meijer, et al. 2020. « PMIF v1.0: Assessing the Potential of Satellite Observations to Constrain CO<sub>2</sub> Emissions from Large Cities and Point Sources over the Globe Using Synthetic Data ». *Geoscientific Model Development* 13 (11): 5813-31. <https://doi.org/10.5194/gmd-13-5813-2020>.

Wang, Yilong, Grégoire Broquet, Philippe Ciais, Frédéric Chevallier, Felix Vogel, Nikolay Kadyrov, Lin Wu, Yi Yin, Rong Wang, et Shu Tao. 2017. « Estimation of observation errors for large-scale atmospheric inversion of CO<sub>2</sub> emissions from fossil fuel combustion ». *Tellus B: Chemical and Physical Meteorology* 69 (1): 1325723. <https://doi.org/10.1080/16000889.2017.1325723>.

Wu, Lin, Grégoire Broquet, Philippe Ciais, Valentin Bellassen, Felix Vogel, Frédéric Chevallier, Irène Xueref-Remy, et Yilong Wang. 2016. « What Would Dense Atmospheric Observation Networks Bring to the Quantification of City CO<sub>2</sub> Emissions? » *Atmospheric Chemistry and Physics* 16 (12): 7743-71. <https://doi.org/10.5194/acp-16-7743-2016>.



## Document History

Version	Author(s)	Date	Changes
	Name (Organisation)	dd/mm/yyyy	
0.0	É Potier (CEA) and all authors	11/01/2021	Initial full draft for circulation
1.0	É Potier (CEA) and all authors	01/02/2021	Consolidated version

## Internal Review History

Internal Reviewers	Date	Comments
Daniel Thiemert (ECMWF)	04/02/2021	Approved

## Estimated Effort Contribution per Partner

Partner	Effort
CEA	12 person-months
<b>Total</b>	12 person-months

This publication reflects the views only of the author, and the Commission cannot be held responsible for any use which may be made of the information contained therein.